I-BAR protein antagonism of endocytosis mediates directional sensing during guided cell migration

Gabriel A. Quinones, Janet Jin, and Anthony E. Oro

Program in Epithelial Biology and Cancer Biology Graduate Program, Stanford University School of Medicine, Stanford, CA 94305

Although directed cellular migration facilitates the coordinated movement of cells during development and repair, the mechanisms regulating such migration remain poorly understood. Missing-in-metastasis (MIM) is a defining member of the inverse Bin/Amphiphysin/Rvs domain (I-BAR) subfamily of lipid binding, cytoskeletal regulators whose levels are altered in a number of cancers. Here, we provide the first genetic evidence that an I-BAR protein regulates directed cell migration in vivo. *Drosophila* MIM (*dmim*) is involved in *Drosophila* border cell migration, with loss of *dmim* function resulting in a lack of directional movement by the border cell cluster. In vivo endocytosis assays combined with genetic analyses demonstrate that the *dmim* product regulates directed cell movement by inhibiting endocytosis and antagonizing the activities of the CD2-associated protein/cortactin complex in these cells. These studies demonstrate that DMIM antagonizes pro-endocytic components to facilitate polarity and localized guidance cue sensing during directional cell migration.

Introduction

Directed cellular migration facilitates the coordinated movement of individual cells, cell clusters, and sheets of cells during development and regeneration. Directed cell migration is important for individual cells as well as groups of cells; there are key differences between these types of migrating cells. Individual cells migrating, either on a plastic dish or in a living tissue matrix, must correctly sense or respond to migratory cues. These cells then undergo changes in their cytoskeletal structure in order to project their cell bodies forward, put down new adhesion complexes, and remove older adhesion complexes at the trailing end of the cell (Harden, 2002; Friedl et al., 2004; Blaser et al., 2005; Montell, 2006; Rørth, 2007). Although cells in a cluster or sheet must also respond to directional cues, they must also maintain the correct cell–cell adhesions and spatial awareness in order to maintain their structure. Directed cluster migration forms the foundation for organ morphogenesis and, when abnormal, has been implicated in disease states such as mental retardation, birth defects, and cancer (Friedl et al., 2004; Kopfstein and Christofori, 2006). Insights into directed cell migration of groups of cells have come from the studies of relatively small clusters of cells, such as border cell migration during *Drosophila* oogenesis (Rørth, 2002; Montell, 2006) or the rearrangement of larger sheets, as is the case during vertebrate gastrulation (Keller, 2005). In *Drosophila* border cell migration, cell clusters initially become autonomously motile, elaborating nondirectional actin-based cellular extensions with little net cellular displacement. Border cell migration is mediated in response to local migratory cues emanating from the ovary via guidance receptors, the *Drosophila* epidermal growth factor receptor (DER) and the PDGF/VEGF-like (PVR) receptor, on the cluster surface. Signaling through the receptors allows border cell membranes to become polarized to form actin-based membrane extensions and migrate along the growth factor gradient (Bianco et al., 2007; Prasad and Montell, 2007). Genetic studies overexpressing DER in border cells indicate that it is not the total levels of receptor, but the location of activated receptors that determines directional migration (Jékely and Rørth, 2003). Despite its importance, our understanding of signaling mechanisms downstream of the guidance receptors that operate in the context of developing organisms remains primitive.

Previous work points to a central role for guidance receptor endocytosis in interpreting local migratory cues to the

G.A. Quinones and J. Jin contributed equally to this paper.

Correspondence to Anthony E. Oro: oro@stanford.edu

Abbreviations used in this paper: BAR, Bin/Amphiphysin/Rvs domain; CD2AP, CD2-associated protein; GMA, GFP fused to the actin-binding domain of moesin; IRS, insulin receptor substrate; MEF, mouse embryonic fibroblast; MIM, missing-in-metastasis; PGC, primordial germ cell; pTyr, phosphotyrosine.

The Rockefeller University Press $30.00
J. Cell Biol. Vol. 189 No. 2 353–367
www.jcb.org/cgi/doi/10.1083/jcb.200910136

underlying cytoskeleton. In cultured mammalian cells, localized receptor-mediated endocytosis and receptor recycling amplifies the guidance signal to focally activate key regulators of the cytoskeleton such as the GTPase Rac1 (Palamidessi et al., 2008). Similar mechanisms appear to control *Drosophila* border cell migration (Jékely et al., 2005; Minina et al., 2007). Forward genetic screens for migration mutants have identified cue-specific components such as the nonreceptor tyrosine kinase Src, components of the endocytic machinery (Jékely et al., 2005; Palamidessi et al., 2008), and the CD2-associated protein (CD2AP)/cortactin complex (Lynch et al., 2003; Somogyi and Rørth, 2004). Each of these components has been shown to regulate endocytosis and cell migration, but little information exists about how they function to regulate directionality during migration.

Increasing attention has been directed toward the Bin/Amphiphysin/Rvs (BAR) superfamily of proteins and their role in endocytosis and vesicle trafficking (Dawson et al., 2006; Frost et al., 2007). Each of the BAR domain subfamilies of curvature-dependent molecular scaffolds are thought to bring together effector complexes to distinct lipid surface in order to regulate actin cytoskeletal remodeling near vesicles. For example, the BAR protein endophilin is critical for early vesicle scission and EGF receptor signaling (Kaneko et al., 2005), and isoforms have been associated with both tumor suppression and oncogenesis. Endophilin is recruited in a receptor-dependent manner through the formation of complexes with the Cbl-associated proteins CIN85 and CD2AP. The endophilin/CD2AP complex in turn mediates vesicle scission through the recruitment of cortactin and the actin-polymerization machinery (Dikic, 2002; Lynch et al., 2003; Kaksonen et al., 2006).

The newest family of BAR domain proteins is the inverse or IMD BAR (I-BAR) family. IMD proteins are defined by the proteins Missing-In-Metastasis (MIM) and the insulin receptor substrate 53 (IRSp53) cytoskeletal regulators (Miki et al., 2000; Lee et al., 2002). MIM was originally identified as a gene whose expression is down-regulated in a variety of urogenital metastatic cancers (Lee et al., 2002; Wang et al., 2007), but other studies have also demonstrated elevated MIM levels in many hedgehog-dependent tumors (Callahan et al., 2004) and metastatic endodermal tumors such as hepatocellular carcinomas (Ma et al., 2007). Like many BAR family proteins, MIM contains several protein–protein interaction modules that suggest it functions to scaffold protein complexes at membranes (Mattila et al., 2003; Woodings et al., 2003; Gonzalez-Quevedo et al., 2005; Lin et al., 2005). Crystal structure analysis indicates that the shape of the IMD dimer is the most convex of the family members thus far, suggesting that the I-BAR family senses a very distinct class of membranes (Lee et al., 2007). I-BAR family members have also been well studied as membrane-deforming proteins with the capacity to cause membrane tubulation and projections (Suetsugu et al., 2006; Mattila et al., 2007; Saarikangas et al., 2008, 2009; Yang et al., 2009). Because each of the other BAR family members has roles in positively regulating endocytosis, the convex shape of the I-BAR proteins is proposed to be involved in antagonizing endocytosis, although this supposition has not been directly tested (Dawson et al., 2006; Lee et al., 2007).

Here, we provide the first in vivo genetic evidence for the involvement of an I-BAR family member in regulating directional migration. We show that MIM and cortactin antagonism underlies a novel molecular steering mechanism.

Results

Vertebrate MIM inhibits endocytosis

Increasing attention has been directed toward the role of the BAR family proteins in endocytosis and vesicle trafficking. Because each subfamily of BAR proteins has been shown to positively regulate endocytosis, we sought to test whether I-BAR proteins function in a similar manner, or because they are structurally distinct from the other families, do they act to antagonize endocytosis. We asked whether MIM, a founding member of the I-BAR family, regulates cell migration and endocytosis using well-characterized, receptor-mediated endocytosis assays in vertebrate cells. Using transferrin endocytosis assays, we found the uptake of HRP-labeled transferrin within 5 min of cell warming to be increased where MIM protein levels are reduced (Fig. 1 A). Similar effects were seen when the kinetics of ^{125}I-labeled EGF uptake were observed after siRNA knockdown of MIM (Fig. 1 B). This effect was not due to altered initial levels of receptor (Fig. 1, F and H). We also observed an increase in recycling levels of both transferrin and EGF (Fig. 1, C and D), consistent with the increase in ^{125}I-EGF uptake. These results indicate that a reduction in MIM protein levels increases endocytosis and recycling, but not receptor degradation, leading us to examine if MIM knockdown alters signaling downstream of the receptor. We tested this by assaying levels of phospho-ERK1/2 (Fig. 1, G and I). In MIM knockdown cells, peak levels of pERK1/2 immunoreactivity remained unchanged, but the duration of the signal persisted twice as long as in control cells. In our short-term cell-based assays we noted no differences in proliferation, adhesion, or overall morphology compared with control-treated cells (not depicted). We also found a marked abnormality in the ability of cells to directionally migrate in response to EGF (Fig. 1 E). From these data we conclude that MIM functions to inhibit receptor-mediated endocytosis, resulting in altered downstream signaling and reduced directional cell migration in vitro.

DMIM is a novel *Drosophila* I-BAR protein

Although MIM is one of the founding members of the I-BAR subfamily of lipid-binding BAR domain proteins, MIM functions have not yet been delineated in vivo, although studies have been conducted with IRSp53 knockout mice (Kim et al., 2009; Sawallisch et al., 2009). Because the BAR subfamilies are represented in Dipterans, we chose to use *Drosophila* to better understand the in vivo roles of these important proteins. *Drosophila* MIM (DMIM, GenBank/EMBL/DDBJ accession no. CG33558) shares strong identity in the I-BAR and WH2 domains with its vertebrate counterpart and ABBA, and less similarity with the I-BAR family member IRS53 (Fig. S1; Scita et al., 2008). Previous structural studies have demonstrated that MIM binds and bends phospholipid-containing membranes (Mattila et al., 2007). To determine whether DMIM retains similar properties,

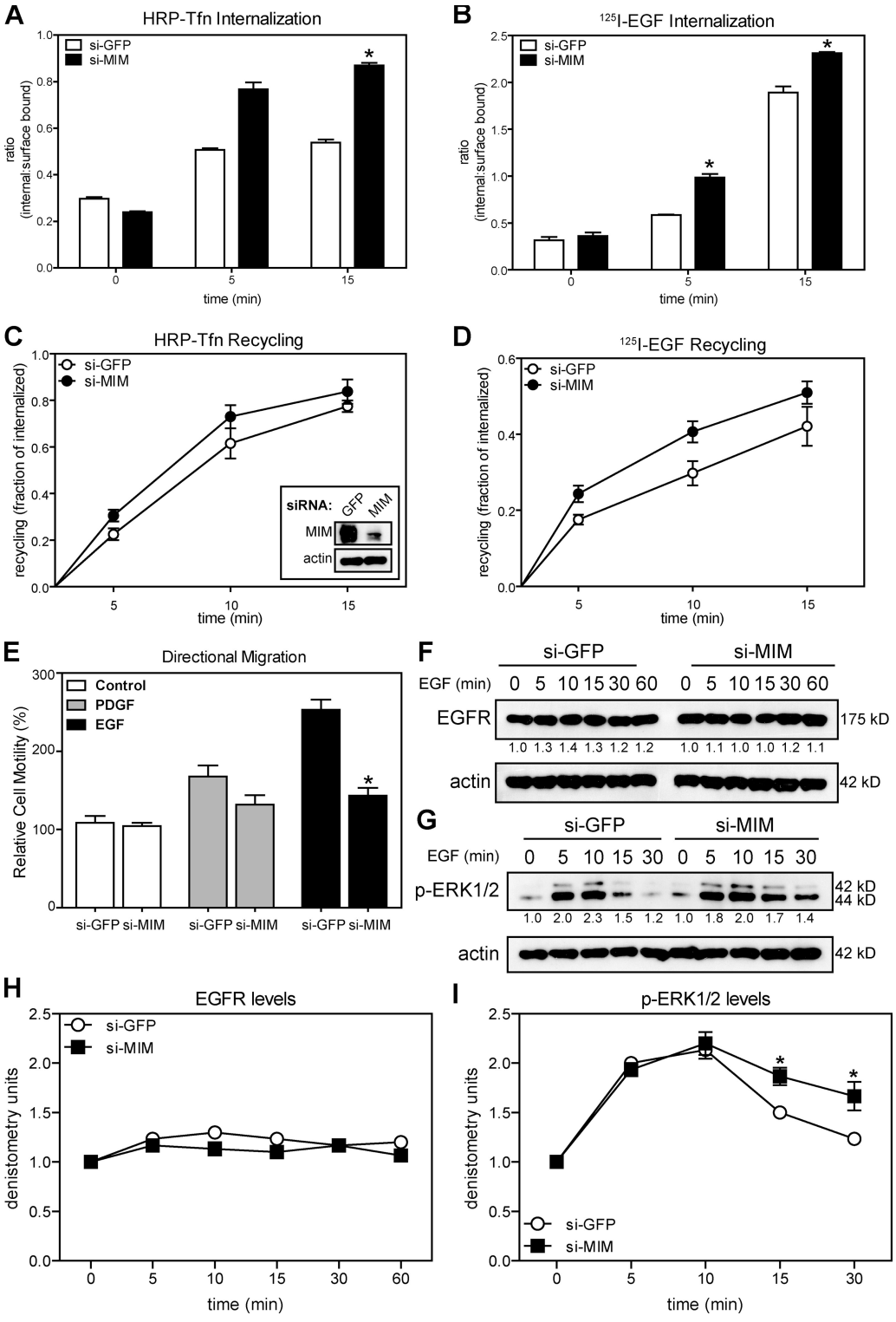

Figure 1. **Vertebrate MIM loss of function results in increased endocytosis and reduced directional migration.** (A and B) Quantification of the ratio of internalized to surface-bound Transferrin (A) of EGF (B) in ptc$^{-/-}$ MEFs treated with indicated siRNAs. Data are represented as the mean ± SEM from three separate experiments (*, $P < 0.01$; *t* test). (C and D) Quantification of the amount of recycled Transferrin (C) or EGF (D) in the medium of ptc$^{-/-}$ MEFs treated with indicated siRNAs. Data are represented as the mean ± SEM from three separate experiments. Inset in C shows immunoblots of protein level knockdown after treatment with indicated siRNAs. (E) MIM knockdown alters EGF-induced directional cell migration. Transwell migration assays showing alterations in the migration of ptc$^{-/-}$ MEFs through a permeable membrane in response to an EGF or PDGF gradient over the course of 8 h. Data are represented as the mean ± SEM from three separate experiments (*, $P < 0.01$; *t* test). (F) EGFR levels in siRNA-treated cells show that si-MIM–treated cells do not display enhanced degradation of the EGF receptor over time. (G) Phospho-ERK1 and 2 levels in cells treated with control or MIM siRNA. MIM knockdown results in prolonged levels of pERK1/2 after the addition of EGF to the cell medium. (H and I) Quantification of immunoblots used for F and G. Data are represented as the mean ± SEM from three separate experiments (*, $P < 0.01$; *t* test).

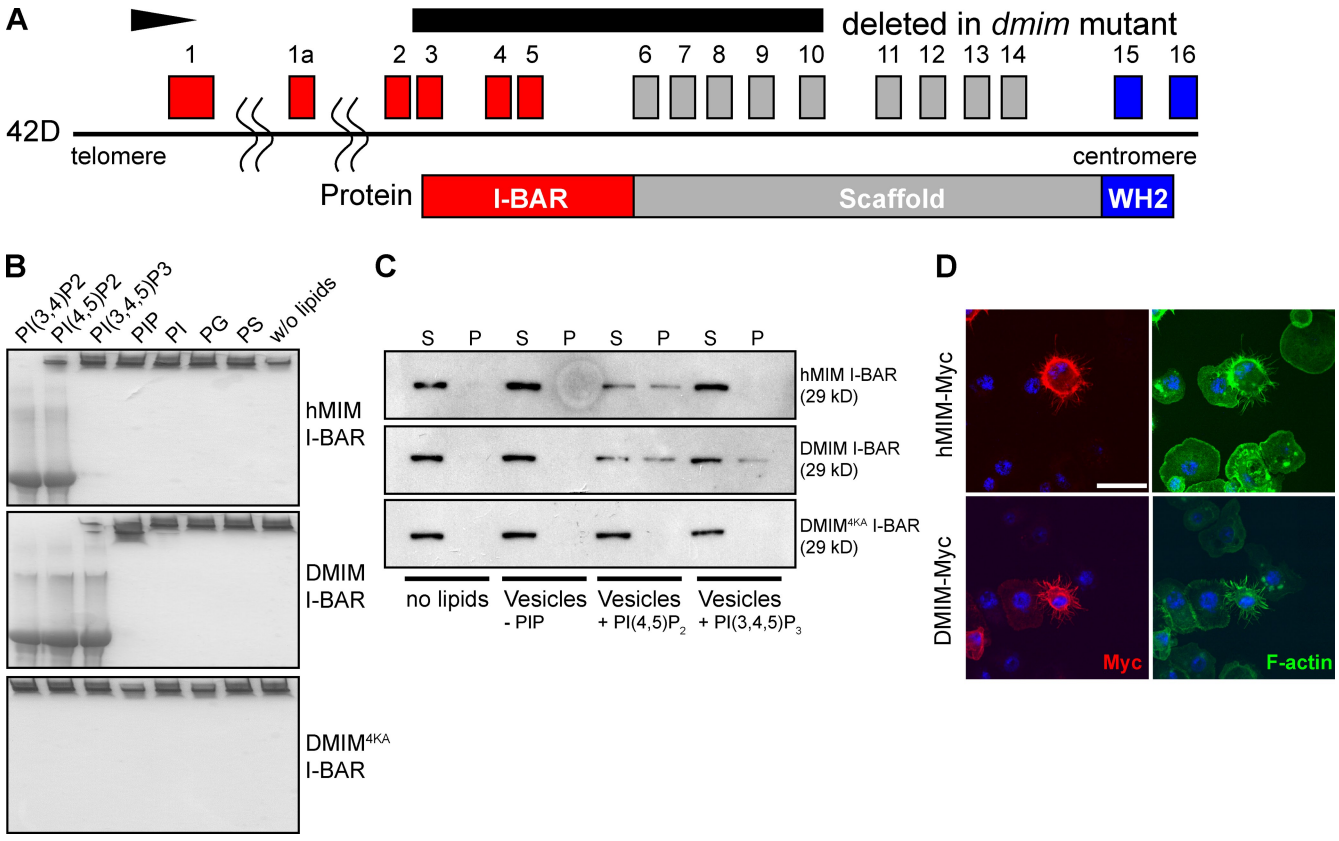

Figure 2. **DMIM is the *Drosophila* homologue of human MIM.** (A) The genomic structure of the *dmim* locus on chromosome 2R, 42C-42E, showing the transcriptional start (arrow) and exons encoding the I-BAR, scaffolding, and WH2 domains. The black box above indicates the exons (3–10) deleted by homologous recombination to make *dmim*-null flies. (B) Native gel of hMIM, DMIM, or DMIM mutant (4KA) I-BAR domains binding with lipids. Only when the I-BAR domain(s) bind to lipids will they run down the native gel. (C) hMIM, DMIM, or DMIM mutant (4KA) I-BAR domain cosedimented with PI(4,5)P2- or PI(3,4,5)P3-rich (30%) large multilamellar vesicles. Human and fly MIM display similar specificity in binding for specific lipids. (D) Overexpressing human or *Drosophila* MIM in *Drosophila* S2 cells results in similar changes in the actin cytoskeleton. Overexpression of either protein results in the formation of actin-based protrusions from the cell membrane. Bar = 20 µm.

we compared the lipid-binding properties of purified fly and human MIM I-BAR domains (Fig. 2, B and C). Both human and DMIM proteins bound to PI(4,5)P2-containing vesicles, whereas the DMIM mutant I-BAR domain failed to bind to these vesicles. The DMIM I-BAR domain was also able to bind to PI(3,4,5)P3-containing vesicles, whereas the human I-BAR was not. This binding was quite specific as mutation of the conserved lipid-binding motifs completely abrogated lipid binding (Mattila et al., 2007). Further, fly or human MIM overexpression in *Drosophila* S2 cells results in the same dramatic cytoskeletal reorientation and extensions (Fig. 2 D), indicating that DMIM functions similarly to its vertebrate orthologue.

Migration defects in *dmim* mutants

To understand the role of DMIM and other I-BAR family members, we generated a *dmim*-null mutant through homologous recombination (Fig. 2 A). We confirmed that the *dmim* mutant lacked the conserved I-BAR domain and much of the scaffolding domain (Fig. S2 A) and *dmim/dmim* phenotypes equaled those from *dmim*/deficiency mothers, arguing the *dmim* mutant is a strong loss-of-function mutant. The *dmim* locus produces a maternal transcript in the ovary, which is then distributed into the germ cells during early embryogenesis (Fig. S2, B–E). Consistent with this maternal expression, *dmim* mutants display partial female sterility (Fig. S2, F and G). *dmim* mutant adults appear phenotypically normal, but display defects in locomotor activity (Fig. S2, H and I). We also observed that *dmim* mutants display marked abnormalities in guided cell migration. Two cell types requiring precise cellular movement during development are the ovarian border cells and the primordial germ cells (PGCs) in the embryo. In the early embryo, PGCs respond to both maternal and zygotic cues from the mesoderm to transmigrate across an epithelial layer toward the genital mesoderm (Kunwar et al., 2006). *dmim* mutant PGCs fail to arrive at the mesodermal target despite apparently normal mesoderm as measured by Clift immunoreactivity (unpublished data). Approximately 10% of the PGCs arrest outside the embryo after germ band extension. Of those that enter, all are capable of transmigration, but only 20% appropriately migrate toward the gonadal mesodermal attractants. The remaining *dmim* PGCs demonstrate a metastatic phenotype, with PGCs scattered throughout the posterior embryo (Fig. 3, A and B).

In the ovary, border cells also perform a well-defined directional migration in response to oocyte-derived growth factor migratory cues (Rørth, 2002; Montell, 2006). The border cell cluster first migrates toward the posterior end of the egg chamber, and then dorsally as the migratory cue changes position. *dmim* mutant border cell clusters have normal numbers and

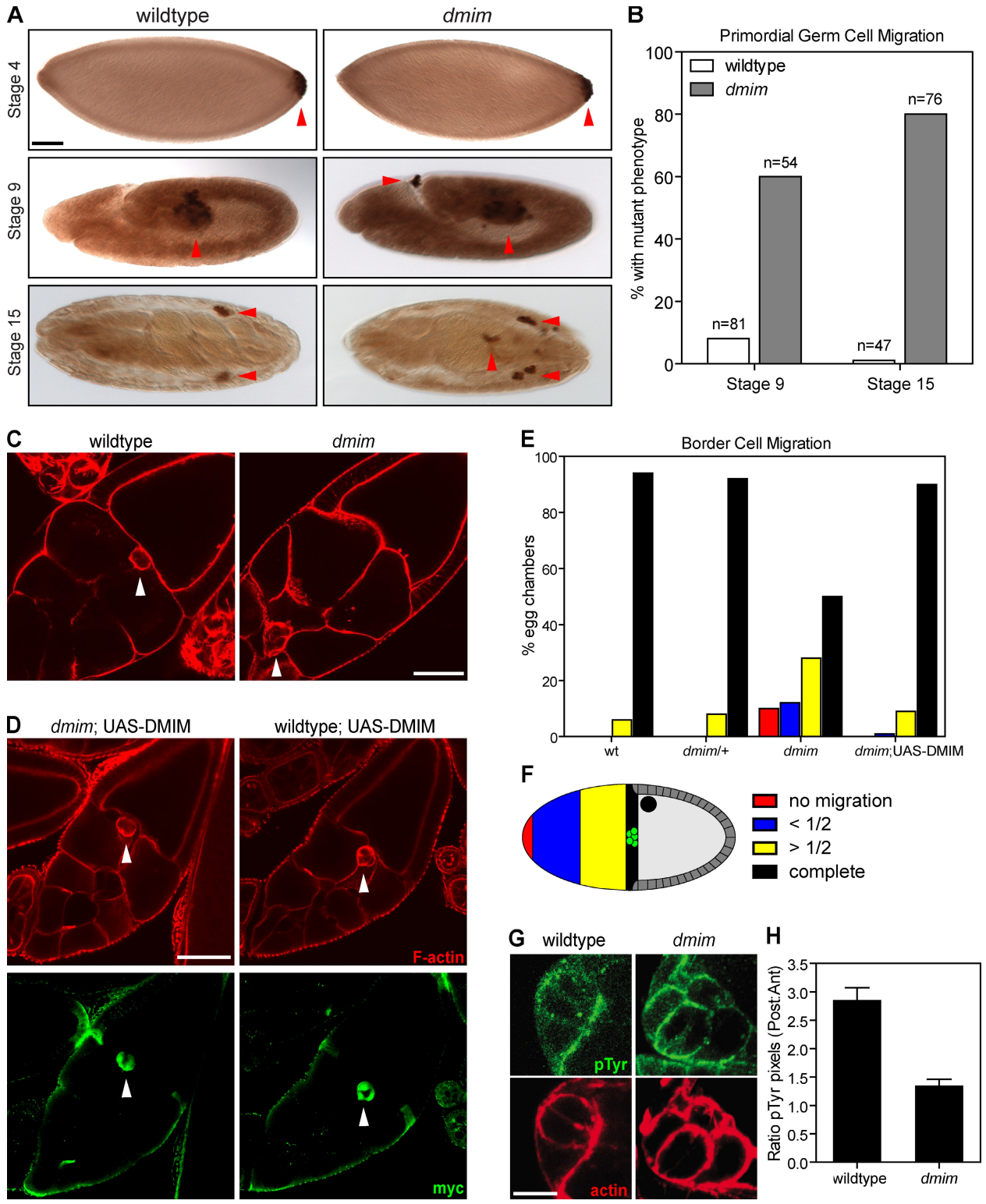

Figure 3. ***dmim*-null flies display abnormal cell migration.** (A) Immunohistochemistry of *Drosophila* embryos at different developmental stages stained with anti-VASA antibody to highlight the progress of germ cell migration. *dmim* mutants display retained germ cells outside of the embryo at stage 9 and mislocalized germ cells in the mesoderm at stage 15. Red arrowheads indicate the position of the primordial germ cells throughout each stage. Bar = 50 µm. (B) Quantification of germ cell migration from two different developmental stages where *dmim* mutants display an aberrant migration pattern. (C) *dmim* mutants are delayed in migration of the border cells in stage 10 egg chambers. The egg chambers are stained with phalloidin (F-actin, red). Bar = 50 µm. (D) Expression of a UAS-DMIM-Myc transgene under the 306-Gal4 driver shows expression of the construct in the border cells in both the *dmim* mutant and wild-type backgrounds. White arrowheads indicate the border cell cluster. Bar = 50 µm. (E) Quantification of border cell migration using the scale described in F; more than 100 egg chambers were examined per genotype. (F) Schematic of a stage 10 egg chamber and scale used to score border cell migration defects. Anterior is to the left. (G) Border cell stained for pTyr (green) and F-actin (red) indicating the portion of the cell membrane where active signaling is occurring. Bar = 5 µm. (H) Quantification of the ratio of posterior to anterior pixel staining with the pTyr antibody. Initial polarized pTyr has been shown to be crucial for proper border cell migration (Jékely et al., 2005).

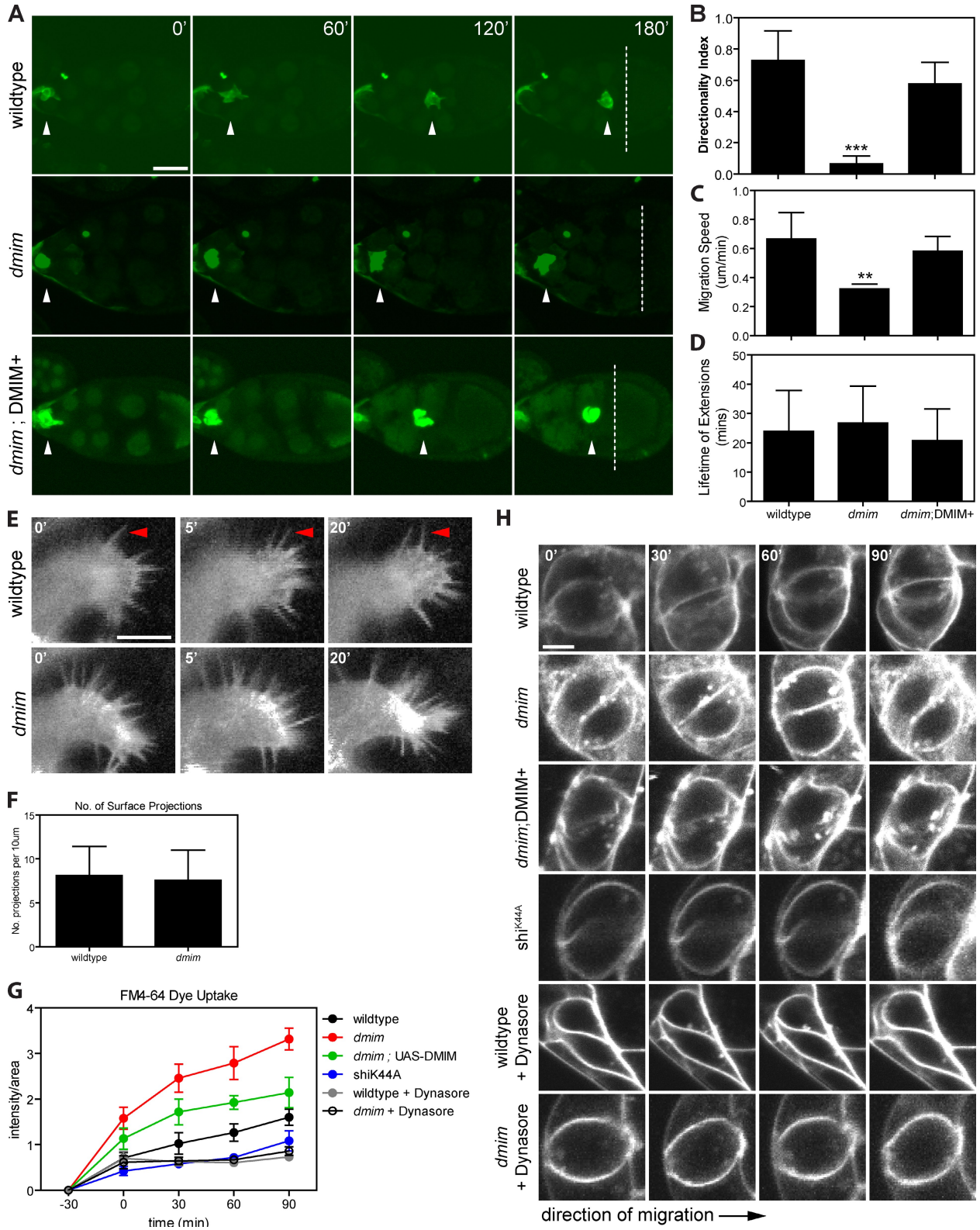

Figure 4. ***dmim* mutants show border cell migration defects and altered endocytosis.** (A) Time-lapse series of confocal micrographs of early stage 9 border cell clusters expressing UAS-GMA under 306-Gal4 in wild-type, *dmim* mutant, and *dmim* mutants expressing UAS-DMIM-Myc transgene in the border cells showing the migration of the border cell clusters over ~3 h. White arrowheads indicate the border cell cluster and the dashed line indicates the anterior end of the oocyte (the end point of border cell migration). Bar = 50 µm. (B) Quantification of the directionality index (DI) of the border cell cluster. The DI is calculated as (A − B)/(A + B), where A is the number of forward extensions and B is the number of rearward extensions. Forward and rearward extensions are defined by which direction they point away from a vertical line on the dorsal ventral axis of the egg chamber. (C) Quantification of the migration speed of the border cell cluster, independent of the direction of migration. (D) Quantification of the average lifetime of each extension from the border cell cluster. All analyses were conducted using five separate movies for each genotype. (**, $P < 0.001$;***, $P < 0.0001$; *t* test). (E) Time-lapse

size (Fig. S3 C), but are significantly delayed in the initial phase of polarized movement compared with their wild-type counterparts. By stage 10, nearly half of the mutant border cells are still delayed, whereas greater than 95% of wild-type clusters have traversed the egg chamber to the oocyte (Fig. 3, C and E).

We focused further on *dmim* function in the border cells because of the ease of genetic manipulation and live imaging in this system. To determine whether the *dmim* product functions in migrating cells or in the surrounding environment, we analyzed the structure of the *dmim* mutant ovary. The polarity, membrane, and cytoskeletal structure appeared to be unaffected as detailed by Fas2, oskar, armadillo, DE-cadherin, and phalloidin immunoreactivity (Fig. S3, A and B). Moreover, expression levels of the migratory cues such as gurken exhibited immunoreactivity comparable to wild type, arguing that *dmim* mutants retain a normal migratory environment. Because the *dmim* locus sits immediately adjacent to recombination sites on the second chromosome, the generation of *dmim* mutants specifically in border cells was not possible. Rather, we aimed to demonstrate cell autonomy by rescuing the *dmim* phenotype through expression of wild-type DMIM in the border cells. Expression of DMIM in border cells resulted in uniform distribution of DMIM protein at both the leading and lagging edges of the migrating border cells (Fig. S3 D). This uniformly distributed expression restored the ability of the cluster to respond to its normal migratory cues (Fig. 3 E). Further, we tested whether higher levels of DMIM expression altered border cell migration using two different lines, the slbo-Gal4 and 306-Gal4 drivers (Fig. S3 D). Gain-of-function *dmim* border cells expressing elevated levels of DMIM protein displayed normal cell shape and border cell migration (Fig. 3 D). Previous studies indicate that membrane response to directional guidance cues are polarized, as measured by phosphotyrosine (pTyr) staining at the leading edge. (Rørth, 2002, 2007; Jékely et al., 2005). *dmim* mutant border cells fail to correctly polarize, as assayed by nonlocalized pTyr staining around the border cell membrane (Fig. 3, G and H). These data suggest that DMIM acts in migrating border and PGC cells to facilitate the initial membrane polarity as the border cells begin to migrate.

dmim mutant border cell migration phenocopies loss of guidance receptors

The study of cell dynamics during migration both in vitro and in vivo has been hampered by the lack of a natural environment to study cell movement or the necessity for fixation to observe the migratory cells. Using recent technical developments that allow live imaging of migrating border cell clusters, we examined the role for *dmim* in border cell motility in a native environment (Bianco et al., 2007; Prasad and Montell, 2007; Tekotte et al., 2007). In vivo cell motility studies have observed three distinct modes of border cell membrane dynamics: initial random extensions independent of cue direction, posterior-directed movement characterized by long extensions toward the guidance cue source, and as the cluster comes closer to the guidance cue source, slower dorsal migration toward the oocyte nucleus. Border cells with constitutively active guidance receptors fail to detach from the anterior chamber and lack cell protrusions, whereas border cells with a lack of guidance receptor activity (i.e., those expressing dominant-negative receptors) have normal cytoplasmic extensions, but lack directional migration (Prasad and Montell, 2007).

To examine how the *dmim* product effects border cell migration, we imaged *dmim* mutant border cells expressing the actin-binding domain of moesin tagged with GFP (GMA) compared with isogenic wild-type controls (Fig. 4 A; Video 1 [wt], Video 2 [*dmim* mutant], Video 3 [*dmim*;DMIM+ rescue]). Using a directional migration index (Prasad and Montell, 2007), we found that wild-type border cells displayed marked directionality toward the cue source, with a directionality index close to 1.0. These data emphasize the marked asymmetry of extensions accompanying normal cluster migration. DMIM depletion impairs the directionality of the border cell cluster (Fig. 4 B), and phenocopies border cell clusters lacking guidance receptors (Prasad and Montell, 2007). Further, we ascertained the duration of the cytoplasmic extensions to determine whether *dmim* had affected the actin cytoskeleton itself. Measurement of the time to maximal extension or retraction in several independent movies clearly indicated no difference in extension lifetime, suggesting that *dmim* is not required for general actin dynamics in these cells in vivo (Fig. 4 D). Because the I-BAR proteins have been shown, when overexpressed, to promote formation of small filopodial-like plasma membrane protrusions in migrating cells, we assayed the number of small cellular projections on the cell surface of individual border cells over time (Fig. 4 E). Similar to our results with larger extensions, we observed no difference in the number of these fine projections (Fig. 4 F). The *dmim* mutants also displayed reduced migration speeds independent of their direction, with *dmim* mutant border cells moving much slower. The average speed for *dmim* mutants was 0.35 µm/min as compared with 0.65 µm/min displayed by wild-type clusters (Fig. 4 C). Expression of DMIM back into the *dmim* mutant border cells (*dmim*;DMIM+) rescues both the directionality index and migration speed phenotypes. Live-cell imaging data in vivo lead us to conclude that DMIM plays a role in properly sensing and responding to directional migratory cues in an otherwise normal migratory environment.

DMIM inhibits endocytosis in border cells

Our in vitro data suggest that MIM inhibition of endocytosis underlies the inability to directionally sense guidance cues. To confirm

series of confocal micrographs of individual border cells expressing UAS-GMA under 306-Gal4. Red arrowheads indicate tracking of a single cellular projection over time. Images were taken every 5 min, and the area shown is a magnification of the leading edge of a single border cell within a migrating cluster. (F) Quantification of the number of small surface projections in E. Data are represented as the mean ± SEM from 10 separate time series for each genotype. (G) Quantification of the amount of FM4-64 dye uptake over time for each indicated genotype. Data are represented as the mean ± SEM from five separate time series for each genotype. (H) Live confocal imaging of border cell clusters stained with the membrane-selective dye FM4-64. Each time series shows the gradual uptake and increase of the dye at the membrane of the border cells. Bar = 5 µm.

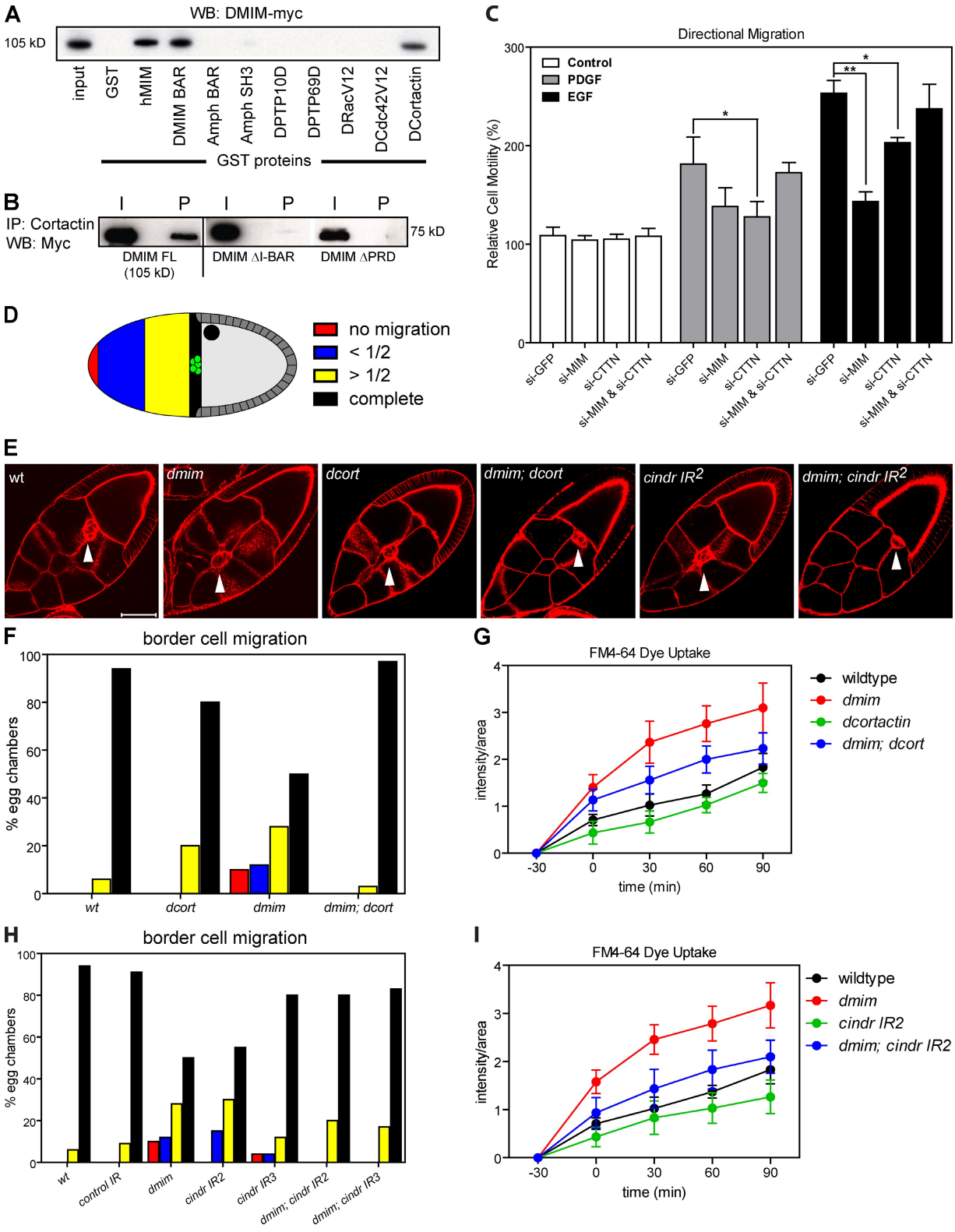

Figure 5. **Loss of *dcortactin* or *cindr* rescues *dmim* border cell migration defects.** (A) GST cosedimentation assay using candidate GST proteins and S2 cell-derived DMIM protein. DMIM binds to itself, human MIM, and DCortactin. (B) Immunoprecipitation assay using an antibody to endogenous DCortactin and lysates from Myc-tagged DMIM constructs. FL (full length DMIM); ΔI-BAR (lacking the IBAR domain); ΔPRD (lacking the polyproline-rich domain). (C) MIM or Cortactin knockdown alters EGF-induced directional cell migration. Transwell migration assays showing alterations in the migration of $ptc^{-/-}$ MEFs through a permeable membrane in response to an EGF or PDGF gradient over the course of 8 h. Data are represented as the mean ± SEM from three separate experiments (*, $P < 0.01$; **, $P < 0.001$; *t* test). (D) Schematic of a stage 10 egg chamber and scale used to score border cell migration defects. Anterior is to the left. (E) Confocal immunofluorescence images of egg chambers from wild-type, *dmim*, *dcortactin*, *dmim; dcortactin*, *cindr* RNAi, and *dmim/cindr* RNAi double-mutant egg chambers stained with phalloidin (F-actin, red). White arrowheads indicate the border cell cluster. Bar = 50 µm. (F and H) Quantification of stage 10 border cell migration for the indicated genotypes; more than 100 egg chambers were examined per genotype.

our in vitro results, we examined border cell membrane dynamics using a live-cell lipophilic dye uptake assay, previously used to measure clathrin-dependent endocytosis rates during *Drosophila* synaptic reuptake (Verstreken et al., 2008). We confirmed the dynamin dependence of dye uptake by showing dramatic reduction of dye uptake in clusters expressing dominant-negative dynamin (slbo-Gal4; shi^{K44A}), or those treated with the dynamin inhibitor Dynasore (Georgiou et al., 2008; Kirchhausen et al., 2008; Fig. 4, G and H). If MIM inhibits receptor-mediated endocytosis, we would expect increased dye uptake in border cells lacking DMIM. During live imaging the dye is taken up throughout the entire egg chamber, including the border cells, and continues to increase after dye addition. However, in *dmim* mutants, the rate of dye uptake compared with wild type was dramatically increased (Fig. 4 G). This effect was not simply due to an increase in general membrane uptake or permeability, as the increased uptake was dynamin dependent and expression of the wild-type DMIM protein in mutant border cells partially rescued the uptake phenotype. The live-cell imaging data, in conjunction with dye uptake studies, support the idea that DMIM regulates guided cell migration through its ability to inhibit receptor-mediated endocytosis.

MIM competes with endophilin/CD2AP for binding to cortactin

BAR domain proteins function through regulating the assembly of protein complexes at membrane surfaces (Ren et al., 2006; Machesky and Johnston, 2007). To understand mechanistically how *dmim* regulates border cell guidance sensing, we sought to discover which proteins, previously known to regulate border cell migration, interact with the scaffolding portion of DMIM. In GST pull-downs and coimmunoprecipitation assays, DMIM formed protein complexes with *Drosophila* cortactin (Dcortactin), but not with Rac1, Cdc42, several RPTPs, and the BAR domain protein amphiphysin (Fig. 5 A). Dcortactin is a major Src phosphorylation target downstream of growth factor signaling and is part of the pro-endocytic complex comprised of the BAR domain protein endophilin and its binding partner CD2AP. The endophilin/CD2AP/cortactin complex helps to provide force for endocytosis and scission of the early endosome by inducing local actin polymerization. Like their vertebrate counterparts, DMIM interacts with Dcortactin through the proline-rich domain (Fig. 5 B). Both MIM and cortactin also affect the directional migration of vertebrate cells in culture. Cells treated with siRNA against either MIM or cortactin display a reduction in cell motility in response of EGF (Fig. 5 C). Simultaneous knockdown of both MIM and cortactin results in normal cell motility, suggesting that these two proteins work antagonistically. The loss of both proteins resulting in a wild-type phenotype also suggests that there is redundancy with another set of proteins with a similar function.

We determined the functional relationship between DMIM and Dcortactin through the examination of border cell phenotypes in double mutants. Previous analysis of *dcortactin* mutants identified a mild border cell migration phenotype (Somogyi and Rørth, 2004), a phenotype we confirmed (Fig. 5, E and F). Surprisingly, we found that *dmim; dcortactin* double mutant border cells do not enhance the mutant phenotype, but rather display a wild-type phenotype. This suggests that DMIM acts antagonistically to Dcortactin to regulate directional cell migration in border cells. Because cortactin is recruited to endophilin via the adapter CD2AP (Dikic, 2002; Soubeyran et al., 2002; Lynch et al., 2003), if the CD2AP/cortactin complex functions antagonistically to MIM in guided migration, then CD2AP mutant border cells should phenocopy *dcortactin* mutants, and also rescue the *dmim* mutant border cell cluster migration phenotype. We assayed the effects of mutations in the single fly CD2AP gene, *cindr*, on border cell migration. Previous studies have indicated that two *cindr^{j}* lines have strong effects on photoreceptor cell morphology (Johnson et al., 2008). We expressed these two independent *cindr^{j}* lines in border cells, where they demonstrated a moderate border cell migration phenotype, mimicking that of *dcortactin* mutants (Fig. 5, E and H). Like *dcortactin*, *cindr^{j}* expression in a *dmim* mutant background partially restores the ability of border cell clusters to migrate, increasing the fraction of clusters that have migrated more than half the distance to the oocyte. We also found that the loss of *dcortactin* or *cindr* results in a mild reduction in the uptake of the FM4-64 dye in border cells (Fig. 5, G and I). As predicted, knockdown of *dmim* in combination with either *dcortactin* or *cindr* results in a partial rescue of the *dmim* increase in dye uptake. From these data, we conclude that the cindr/Dcortactin complex acts to promote endocytosis in opposition to that of DMIM.

Our genetic data suggest guided cell migration is regulated in part from competition for cortactin between the pro-endocytic BAR domain complex endophilin/CD2AP, and the anti-endocytic BAR MIM. To confirm this model, we examined MIM antagonism of cortactin and other endocytic regulators in cultured vertebrate cells to determine whether double mutants would also restore normal receptor uptake in vitro. As predicted, whereas treatment with siRNA against cortactin decreases the levels of EGF receptor endocytosis, siRNA-mediated knockdown of both MIM and cortactin restores receptor uptake levels back to those in the control-treated cells (Fig. 6 A). Consistent with our genetic data, combination knockdowns of MIM with CD2AP also restore EGF uptake levels to control values. We further tested whether MIM antagonism extended to other endocytic regulators. Knockdown of endophilin leads to a reduction in endocytosis with the combined knockdown of endophilin and MIM demonstrating a reproducible trend in elevation of endocytosis over endophilin alone. Knockdown of Cbl, clathrin, or dynamin results in decreased endocytosis and is not

(G and I) Quantification of the amount of FM4-64 dye uptake over time for each indicated genotype. Data are represented as the mean ± SEM from three separate time series for each genotype. Knockdown of *dmim* in combination with either *dcortactin* or *cindr* is able to partially rescue the increase in dye uptake seen in the *dmim* mutant border cells.

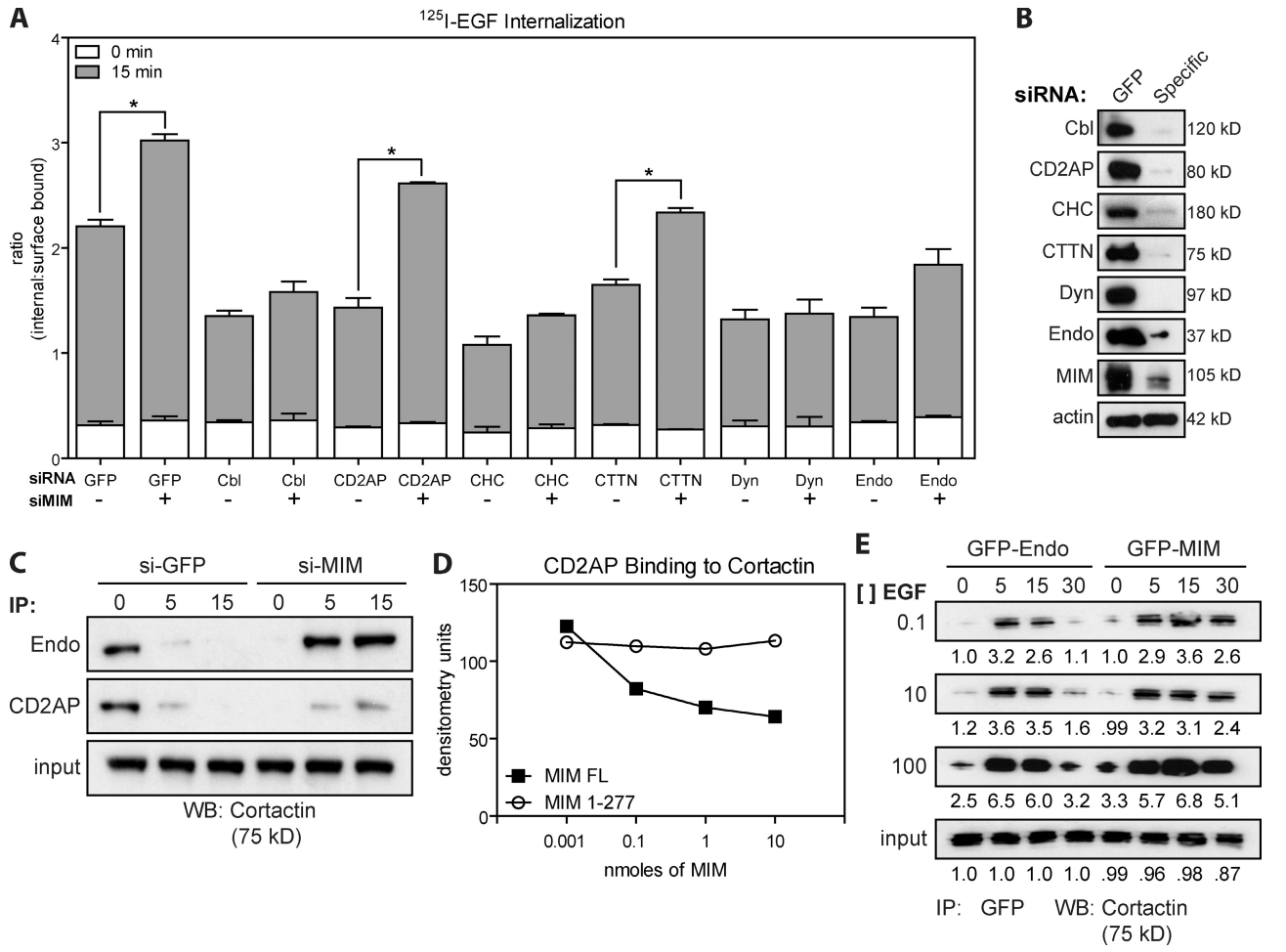

Figure 6. **MIM regulates endocytosis by competing with CD2AP for cortactin binding.** (A) Quantification of the ratio of internalized to surface-bound EGF at 0 and 15 min in ptc$^{-/-}$ MEFs treated with the indicated siRNAs. MIM knockdown shows an increase in EGF uptake, whereas cortactin or CD2AP knockdown shows a decrease in EGF uptake after 15 min. The combination of siRNAs against both MIM and cortactin or MIM and CD2AP restores the phenotype to wild-type levels at 15 min. The phenotype is not restored by simultaneous knockdown with clathrin heavy chain, dynamin, cbl, or endophilin. Data are represented as the mean ± SEM from three separate experiments (*, $P < 0.01$; *t* test). (B) Immunoblots indicating the level of protein knockdown after treatment with siRNAs for A. (C) Coimmunoprecipitations of CD2AP and endophilin with cortactin in si-GFP– or si-MIMtreated ptc$^{-/-}$ MEF lysate showing a decrease in the association of both proteins with cortactin after EGF stimulation. In the si-MIM–treated cells, a prolonged association of CD2AP and endophilin with cortactin is seen when compared with si-GFP–treated cells. (D) Direct competition between in vitro–translated CD2AP and bacterially expressed MIM for the SH3 domain of cortactin. MIM lacking the region that binds cortactin (MIM 1–277) is unable to compete with CD2AP for cortactin binding. (E) Coimmunoprecipitations of GFP-tagged endophilin or GFP-tagged MIM with cortactin in NIH 3T3 cells treated with increasing concentrations of EGF ligand. The interaction between endophilin and cortactin quickly increases within 5 min after stimulation with EGF, and subsequently dissociates within 30 min. The interaction between MIM and cortactin increases within 5 min, but persists strongly even 30 min after stimulation when compared with endophilin.

rescued in combination knockdowns with MIM, suggesting that MIM acts uniquely through CD2AP/cortactin (Fig. 6 A). These results, along with previous studies, suggest that endophilin could be interacting with additional proteins when CD2AP and cortactin are unavailable during EGFR endocytosis (Soubeyran et al., 2002; Schmidt et al., 2003; Kaneko et al., 2005; Gareus et al., 2006; Uezu et al., 2007).

Because circular dorsal ruffles (CDRs) and cortactin have been shown to be an alternative endocytosis pathway for the internalization of growth factor receptors, we investigated MIM and cortactin's role in CDR formation (Lynch et al., 2003; Bompard et al., 2005; Orth et al., 2006; Machesky and Johnston, 2007; Teodorof et al., 2009). In vivo, we found no evidence for CDR formation in migrating border cells. In cultured cells (Fig. S4), we observed that the loss of MIM resulted in a reduction of the CDR formation in response to both PDGF-BB and EGF. However, in contrast to border cells, EGF endocytosis in our MIM and cortactin double mutant cells failed to rescue CDR formation. These results suggest that the effects seen in border cell migration are not a result of increased internalization of the growth factor receptors due to dorsal ruffle formation (Fig. S4 C).

We examined the kinetics of cortactin association with guidance cue addition by performing cortactin immunoprecipitations upon the addition of EGF ligand. Under serum-free conditions, we find that cortactin associates with both endophilin/CD2AP and MIM complexes, but within 5 min after EGF addition, cortactin begins to disassociate from the CD2AP/endophilin complex (Fig. 6 C; Lynch et al., 2003). In the absence of MIM, cortactin fails to dissociate from CD2AP after EGF

addition, resulting in an increase of the amount and duration of endophilin/CD2AP in complex with cortactin (Fig. 6 C). The duration of cortactin association mirrors that of the persistent pERK1/2 immunoreactivity (Fig. 1, H and J). Our work and other studies indicate that both CD2AP and MIM associate through their proline-rich domains with cortactin's SH3 domain (Fig. 5 B; Lynch et al., 2003; Lin et al., 2005). Indeed, in vitro–translated CD2AP readily associates with the purified SH3 domain of cortactin. Increasing concentrations of purified MIM abrogate the binding of cortactin to CD2AP (Fig. 6 D), supporting a direct competition between MIM and CD2AP for cortactin binding. MIM lacking its proline-rich domain (MIM 1–277) fails to compete with CD2AP, providing additional support for the idea that MIM antagonizes the ability of cortactin to associate with the pro-endocytic CD2AP/endophilin complex. We then used stable GFP-tagged MIM and endophilin lines to examine cortactin association with each of the proteins at different EGF ligand concentrations over time. The antagonism between MIM and CD2AP/endophilin for cortactin binding could be explained by the prolonged association between cortactin and MIM, which persists longer after stimulation with EGF ligand than the association between endophilin and cortactin, even at different ligand concentrations (Fig. 6 E).

Discussion

We have shown through genetic interaction and live-cell imaging that migrating cells use a MIM-dependent steering mechanism to interpret local migratory signals. MIM's role appears to be general, as both border cell and PGC migration are affected in *dmim* mutants and involve different cell types responding to different guidance cues. Our data indicate that MIM inhibits guidance receptor endocytosis by competing directly with CD2AP for cortactin, resulting in dampened guidance receptor signaling. This study provides the first genetic and biochemical evidence for the function of a member of the I-BAR family of proteins in directed cell migration, and provides a mechanistic link between MIM and cell migration.

Directional cell migration is a complex process requiring dynamic rearrangements of the cytoskeleton and precise directional sensing of local migratory cues (Prasad and Montell, 2007). Our live-cell imaging data suggest that DMIM is involved in directing cell migration through the inhibition of endocytosis. Although previous studies demonstrate that MIM is an actin cytoskeletal remodeling protein (Gonzalez-Quevedo et al., 2005; Lee et al., 2007; Mattila et al., 2007), our imaging studies argue against a major, direct role for MIM in general actin polymerization. Consistent with this notion is the lack of apparent defects in adherens junctions, the actin cytoskeleton, or anteroposterior polarity in *dmim* mutant egg chambers. This is not to say that MIM does not affect the actin cytoskeleton in other cases of cell migration, just that in the case of *Drosophila* border cell migration the function of DMIM is not required for actin cytoskeletal dynamics. Previous studies have also implicated MIM in regulating Sonic Hedgehog signaling (Callahan et al., 2004). Mutations in the hedgehog pathway component costal2 result in aberrant border cell numbers (Liu and Montell, 1999), but *dmim* mutants display a wild-type number of border cells. This discrepancy could be explained in part due to the observation that MIM associates with vertebrate Suppressor of Fused (Callahan et al., 2004), which is redundant in flies. The data presented here uncover migratory defects in PGCs, border cells, and vertebrate cultured fibroblasts, all responding to different migratory cues. This suggests that although cells use different cues and receptors for migration in a variety of systems, the regulation of this process at the level of endocytosis appears to be shared.

Our studies identify DMIM as novel I-BAR protein, and one of the first negative regulators of endocytosis with a role in guided cell migration. Genetic, cell biological, and biochemical data support the model that DMIM and CD2AP compete for cortactin in regulating receptor-mediated endocytosis. The observation that removing both MIM and cindr/cortactin results in wild-type migration suggests that MIM and cortactin constitute one of several redundant regulatory systems to control the directional migration of the border cells. Because removal of both proteins restores normal border cell migration but disruption of clathrin and dynamin function does not, we speculate that other combinations of pro- and anti-endocytosis complexes downstream of dynamin must be operating to balance this process in migrating cells. Although we see a trend in increased endocytosis with MIM/endophilin double knockdown, the lack of complete rescue further suggests endophilin possesses MIM-independent endocytosis functions. Current studies are ongoing to identify these additional signaling pathways in the sensitized *dmim*;*dcortactin* background. More importantly, our data show the dramatic effects on migration when components of the steering mechanism are missing or out of balance. Similar effects have also been seen with gross overexpression of cortactin (Timpson et al., 2005) and may explain the relatively high frequency of cortactin and MIM alterations in late-stage cancers (Patel et al., 1996; Lee et al., 2002; Timpson et al., 2007; Hofman et al., 2008).

These results provide a new mechanistic understanding of BAR domain function by showing that directional sensing comes in part from protein complexes competing for common effector proteins during endocytosis. These data support the notion that MIM acts to dampen guidance receptor signaling at a variety of ligand concentrations by sequestering cortactin. Guidance cue binding assembles the N-BAR subfamily member endophilin and its adapter CD2AP, which binds cortactin, shifting it away from MIM sequestration. We postulate that increased endocytosis and MIM's persistent binding of cortactin prevent the cell from improperly sensing guidance cues and misinterpreting directional differences. Previous studies suggest that phosphorylation of cortactin modulates its interaction with a number of proteins (Zhu et al., 2007); however, we do not detect such alteration using phosphospecific cortactin antibodies in our system (unpublished data). Consistent with this data are the lack of localized bulk MIM protein at the leading edge of cultured cells or rescued *dmim*; DMIM+ border cells. Altogether, these data suggest that there is a novel MIM-dependent steering mechanism that guides cell migration through interactions with other protein complexes. Jékely et al. (2005)

demonstrated the importance for regulating both polarity and a localized response to external stimuli during the migration of the border cell cluster. Their studies focused on regulation of receptor tyrosine kinase signaling through the action of key proteins involved in the endocytosis of the receptor. We have focused our studies on a negative regulator of endocytosis, which in the *Drosophila* border cell cluster regulates both polarity and a local response to guidance cues as a means of mediating directional migration.

Materials and methods

Transferrin internalization and recycling

Ptc1-null mouse embryonic fibroblasts (MEFs; Taipale et al., 2000) were used throughout these studies due to the increased levels of MIM protein expressed when compared with NIH 3T3 cells, as well as the ease of MIM knockdown at the protein level in these cells. Ptc1-null MEFs were nucleofected with the appropriate siRNA 2 d before the endocytosis assays, and were serum starved overnight before the assays. Endocytosis was measured using HRP-conjugated mouse Transferrin (Tfn; Sigma-Aldrich) and detected using a Sensolyte ADHP HRP ELISA Assay kit (AnaSpec). To measure the amount of internalized HRP-Tfn, cells were serum starved overnight, the HRP-Tfn (100 µg/ml) in serum-free DME was added to each well, and the plate was placed at 37°C for the indicated time(s). Endocytosis was stopped by placing the plate on ice, washing with ice-cold PBS, pH 5.0, for 2 min each, and then 4 times with PBS, pH 7.0. The cells were then lysed in 20 mM Hepes, pH 7.9, 150 mM NaCl, and 1% NP-40 for 10 min on ice. The amount of HRP-Tfn in the lysate was then measured following the Sensolyte kit protocol. To measure recycling of HRP-Tfn, cells were treated as per the above protocol. After stripping the unbound ligand from the cell surface, fresh serum-free medium was placed on the cells. Medium was then collected from the wells at the indicated time points and assayed for HRP-Tfn content following the Sensolyte kit protocol.

EGF stimulation, internalization, and recycling

For the EGF stimulation, Ptc1-null MEFs were grown for 2 d after nucleofection and then serum starved overnight. Cells were stimulated with EGF at 100 ng/ml (Sigma-Aldrich) in serum-free DME for the indicated times, washed twice with PBS, and lysed. Lysates were loaded onto SDS-PAGE gels for Western blot analysis. The primary antibodies used were: rabbit anti-cortactin (1:1,000; Millipore), mouse anti–β-actin (1:10,000), rabbit anti-MIM (1:500), mouse anti-CD2AP (1:500; Santa Cruz Biotechnology, Inc.), mouse anti-endophilin (1:1,000; Abcam), rabbit anti-dynamin (1:1,000; Abcam), rabbit anti-clathrin heavy chain (1:1,000; Abcam), and goat anti-CBL (1:1,000; Abcam).

For ^{125}I-EGF assays, ptc1-null cells were grown for 2 d after nucleofection and then serum starved overnight. After serum starvation, the cells were stimulated with EGF (100 ng/ml) in serum-free DME for the indicated times. Radiolabeled EGF at 1 ng/ml, (NEX1600; PerkinElmer) was combined with unlabeled EGF to a final concentration of 100 ng/ml. For internalization assays, unbound ligand was removed by washing three times with ice-cold buffer containing: 20 mM Hepes, 130 mM NaCl, 5 mM KCl, 0.5 mM $MgCl_2$, 1 mM $CaCl_2$, and 1 mg/ml polyvinylpyrolidione, pH 7.4. Surface-bound ligand was then collected in ice-cold acid strip buffer (50 mM glycine-HCl, 100 mM NaCl, and 1 mg/ml polyvinylpyrolidione, pH 3.0) for 2 min. Internalized ligand was then released with 5 N NaOH for 30 min, added to reducing sample buffer, and analyzed with a scintillation counter. For recycling assays, unbound ligand was removed as described above, then fresh serum-free medium was added to the cells. The cells were placed at 37°C for the indicated times. At each time point, medium was removed from the well and assayed for EGF content. Results were normalized to the initial amount of EGF in the medium at time 0. All siRNAs were ordered from Thermo Fisher Scientific; si-MIM: 5′-GCAAGGCACUCAUCGAAGAUU-3′, ON-TARGETplus SMARTpool siRNAs were used for: Cbl, CD2AP, clathrin, cortactin, dynamin, and endophilin.

Fly genetics

The *dmim* mutant was made using a modified version of "ends-out" homologous recombination (Gong and Golic, 2003). The donor vector was constructed by cloning PCR products of the homologous regions in the *dmim* genomic region upstream and downstream of the deleted exons (exons 3–10) into the pP[EndsOut2] vector (a gift from Dr. Jeff Sekelsky, University of North Carolina, Chapel Hill, NC). The primers used were, 5′-CCCGGGAGCGAGTGAGGACGCGCAAATGG-3′ and 5′-GGTACCGACCAGTTCCTGGGCCACAGAC-3′ to amplify the 5′ region and 5′-AGATCTAGTCAGGTGAGAGTAGGAAATC-3′ and 5′-GAATTCCTGCCACACGCTCCCATTCCATATCC-3′ to amplify the 3′ region. Mutant chromosomes were out crossed to yw flies for five generations to minimize linked enhancers and suppressors. DMIM rescue lines were made by cloning the *dmim* cDNA into the pUAST or pUASp vectors with a myc-his epitope tag on the C terminus. Transgenic lines were generated using standard methods. Transgenic lines were crossed into the 306-Gal4 (Bloomington Drosophila Stock Center, Bloomington, IN) for expression in the border cells. The slbo-Gal4 and shi^{K44A} lines were obtained from the Bloomington Drosophila Stock Center. UAS-*cindr*-IR$^{2.21A + 2.23A}$ (*cindr* IR^2) targets the long and intermediate *cindr* transcripts and UAS-*cindr*-IR$^{3.73B + 3.81A}$ (*cindr* IR^3) targets all three transcripts, as described previously (Johnson et al., 2008). The Cortactin^{M7} line has been described previously (Somogyi and Rørth, 2004).

In vitro migration assays

For directional cell migration assays in vitro, cells were seeded into the upper compartment of a Transwell 12-well plate (Costar 3403; Corning) in serum-free medium after 16 h of serum starvation. The lower compartment of each well contained serum-free medium with or without the indicated growth factor. Cells were allowed to migrate for 8 h, then the medium was removed and the cells were fixed with 4% paraformaldehyde. Fixed cells were stained with 0.5% crystal violet and the cells in the upper compartment were scraped off of the insert membrane. The well was then extensively washed with water and allowed to air dry. Only cells that migrated down through the porous membrane remained. The crystal violet remaining in these cells was then extracted with 30% acetic acid and assessed by measuring the absorbance at 590 nm.

Lipid vesicle cosedimentation assays

6XHis fusion proteins of DMIM I-BAR (aa 1–477), hMIM I-BAR (aa 1–255), and DMIM^{4KA} I-BAR were cloned by standard techniques in pQE80L vector, expressed in bacteria and purified on Superflow Nickel Beads (QIAGEN). DMIM^{4KA} contained mutations K139A, K140A, K149A, and K150A generated by QuikChange Mutagenesis (Stratagene). PI(4,5)P_2 (L-α-phosphatidylinositol-4,5-bisphosphate; porcine brain, tri-ammonium salt), PI(3,4,5)P_3 (1,2-dileoyl-*sn*-glycero-3-[phosphoinositol-3,4,5-trisphosphate], tetra-ammonium salt), phosphatidylserine (PS; brain), phosphatidylcholine (PC; brain), and phosphoethanolamine (PE) were purchased from Avanti Polar Lipids, Inc. Fusion proteins were diluted to desired concentrations in F-buffer (10 mM imidazole, pH 7.5, 0.2 mM $CaCl_2$, 0.2 mM ATP, 1 mM DTT, 100 mM KCl, 2 mM $MgCl_2$, and 1 mM EGTA). For vesicle cosedimentation assays the following mixtures were prepared: 5% PE, 20% PS, 45–75% PC, and 0–30% PI(4,5)P_2 or PI(3,4,5)P_3. Samples were vacuum dried under N_2 and hydrated for a minimum of 4 h in 0.2 mM Hepes-KOH, pH 7.5, and 100 mM NaCl to a 1-mM total lipid concentration. Large multilamellar vesicles were formed by repeated freeze/thaw cycles between liquid nitrogen and a hot water bath. Vesicles were also vortexed before each experiment. I-BAR constructs were diluted in desired concentrations in F-buffer and sedimented at 360,000 *g* for 30 min at room temperature. For native gel electrophoresis, fusion proteins were diluted to desired concentration in F-buffer. Lipid/protein reactions were incubated at room temperature for 1 h, run on 12% native PAGE gels, stained with Coomassie, and scanned.

***Drosophila* egg chamber immunofluorescence**

For confocal immunofluorescence, ovaries from 1–2-d-old females were dissected in PBS, fixed, and permeabilized in 4% paraformaldehyde and PBSX (0.1% Triton X-100) for 20 min at room temperature and subsequently washed in PBSX, blocked in 5% normal horse serum (Vector Laboratories), and then incubated overnight in primary antibody at 4°C. The primary antibodies used were: mouse anti-armadillo (1:200; Developmental Studies Hybridoma Bank [DSHB], Iowa City, IA), mouse anti-Myc (1:100; Sigma-Aldrich), phalloidin-AF633 (1:100; Invitrogen), mouse anti-DE cadherin (1:250; DSHB), mouse anti-oskar (1:250; DSHB), mouse anti-lectin FITC (1:250; Vector Laboratories), mouse anti-FasIII (1:500; DSHB), mouse anti-gurken (1:100; DSHB), rabbit anti-DCortactin (1:250; a gift from Dr. Togashi, Tohoku University, Sendai, Japan), mouse anti-GFP (1:250; Sigma-Aldrich), and phalloidin-TRITC (1:100; Sigma-Aldrich). Alexa Fluor–conjugated antibodies (Invitrogen) were used as secondaries.

***Drosophila* egg chamber live imaging**

For live confocal imaging, egg chambers from ovaries were prepared according to previous protocols (Bianco et al., 2007; Prasad and Montell, 2007; Tekotte et al., 2007) with some modification. Egg chambers were

placed in Petri dishes with glass coverslip bottoms (MatTek), surrounded by halocarbon oil 700 (Sigma-Aldrich) and covered by the gas-permeable membrane from a Petriperm plate (Grenier Bio). Females were taken 1–3 d after eclosion and fed fresh yeast 1 d before dissection. Dissections were performed in Schneider's Insect medium (Invitrogen) supplemented with 15% fetal bovine serum (Sigma-Aldrich), 0.20 mg/ml^{-1} insulin (Sigma-Aldrich), 0.6x penicillin/streptomycin (Invitrogen), and 3 mM FM4-64 (Invitrogen). Ovaries were removed, washed in dissection medium, and individual ovarioles were removed from the muscle sheath using fine dissection forceps. Imaging was performed using a microscope (LSM-510 Meta; Carl Zeiss, Inc.) with a 340 1.3 NA Plan NeoFluor oil immersion objective. Two channels were acquired simultaneously: GFP (488-nm laser and 500–550-nm band-pass filter) and FM4-64 (488-nm laser and 560-nm long-pass filter). 7 sections were taken 5 µm apart with 5 min between stacks. The three to four sections covering the migrating cluster were merged for each time point using the Volocity 4 imaging software package (PerkinElmer). Videos were made using Volocity 4, and exported as QuickTime (.mov) files at 5 frames per second. Egg chambers were chosen in which border cells had clearly delaminated or were already migrating. For dye uptake assays, egg chambers were incubated in 9 µM FM4-64 dye in imaging medium for exactly 30 min before the first image was taken. For Dynasore (Sigma-Aldrich) inhibition of dynamin in the egg chambers, dissected egg chambers were incubated in imaging medium containing 80 µM Dynasore for 1 h before the addition of FM4-64.

Live imaging calculations

The directionality index (DI) for large cellular extensions emanating from a border cell is calculated as (A − B)/(A + B), where A is the number of forward extensions and B is the number of rearward extensions. Forward and rearward extensions are defined by which direction they point away from a vertical line on the dorsal ventral axis of the egg chamber. For the purposes of this study, cell extensions are defined as transient, large cellular processes that are greater than one quarter of a border cell diameter in width at their base, and extend outward from the cell surface. Cellular filopodial-like projections are defined as cellular processes that are transient, less than one quarter of a cell diameter in width at the base, and extend from the cell surface. Tracking of cellular extensions/projections was performed using the tracking module of the Volocity program. Each individual process was manually marked and tracked throughout each frame to calculate the amount of time each process persisted. The number of projections was calculated by counting the number of projections along a 10-µm length of cell surface along a border cell. We are limited in the types of projection studies as our analyses cannot account for projections that form and dissociate faster than the 5-min time points collected. For FM4-64 dye uptake assays, images were taken over time of the border cell cluster and analyzed using ImageJ. A line drawn following the outside of the membrane of a single border cell was used to select the area from which the intensity measurements were calculated. The intensity measurement was then divided by the area selected to control for normal variations in border cell shapes and sizes. These analyses were all normalized to the overall intensity of the entire egg chamber to account for differences in uptake throughout the egg chamber itself. Measurements from single border cells within the same cluster were combined with measurements from cells of a different cluster for both technical and biological replicates within the analyses. A mutant dynamin (shi^{K44A}) and a small molecule inhibitor of dynamin were included as negative controls to show that dye uptake is dependent on clathrin-mediated endocytosis, and not just accumulation of the dye in the membrane over time.

GST pull-downs and coimmunoprecipitations

For GST pull-downs, cells were lysed in PBS with 1% NP-40, protease inhibitors, 1 mM Na_3VO_4, and 5 mM NaF for 30 min at 4°C. For coimmunoprecipitations, cell lysates were generated using RIPA buffer (50 mM Tris-HCl, pH 8.0, 150 mM NaCl, 5 mM EDTA, 1% NP-40, 0.1% SDS, 10% glycerol, 0.5% Na deoxycholate, 1 mM Na_3VO_4, and protease inhibitors) and precleared with Protein G PLUS-Agarose beads (Santa Cruz Biotechnology, Inc.) for 30 min at 4°C. The primary antibodies used were: rabbit anti-cortactin (1:1,000; Millipore), rabbit anti-MIM (1:500), mouse anti-CD2AP (1:500; Santa Cruz Biotechnology, Inc.), goat anti-endophilin I (1:500; Santa Cruz Biotechnology, Inc.), mouse anti-Myc (1:500; Sigma-Aldrich), and rabbit anti-Myc (1:1,000; Santa Cruz Biotechnology, Inc.).

Direct binding and competition assays

The coding sequence of CD2AP was cloned into pcDNA3.1 MHA. CD2AP protein was made using a TNT T7 Coupled Reticulocyte Lysate System (Promega). GST beads containing the SH3 domain of cortactin were incubated with equal amounts of CD2AP and increasing amounts of bacterially expressed full-length 6X-His MIM protein or 6X-His MIM lacking the C-terminal proline-rich domain. The beads were washed with PBST and run on SDS-PAGE gels for Western blot analysis using rabbit anti-CD2AP (1:500; Cell Signaling Technology).

Online supplemental material

Fig. S1 shows ClustalW2 alignment of the I-BAR and WH2 domain of *Drosophila*, human, and mouse MIM as well as mouse ABBA and mouse IRSp53. Fig. S2 shows eclosion and hatching frequency deficiencies in *dmim* mutants as well as locomotor defects in the adults. Fig. S3 shows a comparison of staining patterns of cell–cell junctions, membranes, growth factor gradients, and the actin cytoskeleton between wild-type and *dmim* mutant egg chambers. Fig. S4 shows the effect of MIM knockdown on the formation of circular dorsal ruffles in vertebrate cell culture. Video 1 shows wild-type border cells migrating normally toward the oocyte (right). Video 2 shows *dmim* mutant border cells fail to migrate toward the oocyte (right). Video 3 shows *dmim*/DMIM+ border cells migrating normally toward the oocyte (right). Online supplemental material is available at http://www.jcb.org/cgi/content/full/jcb.200910136/DC1.

We wish to thank P. Rorth, J. Sekelsky, and D. Kiehart for flies and plasmids; R. Johnson and R. Cagan for the *cindr* RNAi fly lines; P. Khavari, H. Chang, and S. Pfeffer for comments on the work; M. Bershteyn for MIM siRNA sequences; and L. Edgington and A. Bailey for technical support.

This work was supported by NSF predoctoral fellowships to G.A. Quinones and J. Jin, and an NIH/NIAMS grant to A.E. Oro (R01 AR052785).

Submitted: 23 October 2009
Accepted: 19 March 2010

References

Bianco, A., M. Poukkula, A. Cliffe, J. Mathieu, C.M. Luque, T.A. Fulga, and P. Rørth. 2007. Two distinct modes of guidance signalling during collective migration of border cells. *Nature.* 448:362–365. doi:10.1038/nature05965

Blaser, H., S. Eisenbeiss, M. Neumann, M. Reichman-Fried, B. Thisse, C. Thisse, and E. Raz. 2005. Transition from non-motile behaviour to directed migration during early PGC development in zebrafish. *J. Cell Sci.* 118:4027–4038. doi:10.1242/jcs.02522

Bompard, G., S.J. Sharp, G. Freiss, and L.M. Machesky. 2005. Involvement of Rac in actin cytoskeleton rearrangements induced by MIM-B. *J. Cell Sci.* 118:5393–5403. doi:10.1242/jcs.02640

Callahan, C.A., T. Ofstad, L. Horng, J.K. Wang, H.H. Zhen, P.A. Coulombe, and A.E. Oro. 2004. MIM/BEG4, a Sonic hedgehog-responsive gene that potentiates Gli-dependent transcription. *Genes Dev.* 18:2724–2729. doi:10.1101/gad.1221804

Dawson, J.C., J.A. Legg, and L.M. Machesky. 2006. Bar domain proteins: a role in tubulation, scission and actin assembly in clathrin-mediated endocytosis. *Trends Cell Biol.* 16:493–498. doi:10.1016/j.tcb.2006.08.004

Dikic, I. 2002. CIN85/CMS family of adaptor molecules. *FEBS Lett.* 529:110–115. doi:10.1016/S0014-5793(02)03188-5

Friedl, P., Y. Hegerfeldt, and M. Tusch. 2004. Collective cell migration in morphogenesis and cancer. *Int. J. Dev. Biol.* 48:441–449. doi:10.1387/ijdb.041821pf

Frost, A., P. De Camilli, and V.M. Unger. 2007. F-BAR proteins join the BAR family fold. *Structure.* 15:751–753. doi:10.1016/j.str.2007.06.006

Gareus, R., A. Di Nardo, V. Rybin, and W. Witke. 2006. Mouse profilin 2 regulates endocytosis and competes with SH3 ligand binding to dynamin 1. *J. Biol. Chem.* 281:2803–2811. doi:10.1074/jbc.M503528200

Georgiou, M., E. Marinari, J. Burden, and B. Baum. 2008. Cdc42, Par6, and aPKC regulate Arp2/3-mediated endocytosis to control local adherens junction stability. *Curr. Biol.* 18:1631–1638. doi:10.1016/j.cub.2008.09.029

Gong, W.J., and K.G. Golic. 2003. Ends-out, or replacement, gene targeting in *Drosophila*. *Proc. Natl. Acad. Sci. USA.* 100:2556–2561. doi:10.1073/pnas.0535280100

Gonzalez-Quevedo, R., M. Shoffer, L. Horng, and A.E. Oro. 2005. Receptor tyrosine phosphatase-dependent cytoskeletal remodeling by the hedgehog-responsive gene MIM/BEG4. *J. Cell Biol.* 168:453–463. doi:10.1083/jcb.200409078

Harden, N. 2002. Signaling pathways directing the movement and fusion of epithelial sheets: lessons from dorsal closure in *Drosophila*. *Differentiation.* 70:181–203. doi:10.1046/j.1432-0436.2002.700408.x

Hofman, P., C. Butori, K. Havet, V. Hofman, E. Selva, N. Guevara, J. Santini, and E. Van Obberghen-Schilling. 2008. Prognostic significance of cortactin levels in head and neck squamous cell carcinoma: comparison with epidermal growth factor receptor status. *Br. J. Cancer.* 98:956–964. doi:10.1038/sj.bjc.6604245

Jékely, G., and P. Rørth. 2003. Hrs mediates downregulation of multiple signalling receptors in *Drosophila*. *EMBO Rep.* 4:1163–1168. doi:10.1038/sj.embor.7400019

Jékely, G., H.H. Sung, C.M. Luque, and P. Rørth. 2005. Regulators of endocytosis maintain localized receptor tyrosine kinase signaling in guided migration. *Dev. Cell.* 9:197–207. doi:10.1016/j.devcel.2005.06.004

Johnson, R.I., M.J. Seppa, and R.L. Cagan. 2008. The *Drosophila* CD2AP/CIN85 orthologue Cindr regulates junctions and cytoskeleton dynamics during tissue patterning. *J. Cell Biol.* 180:1191–1204. doi:10.1083/jcb.200706108

Kaksonen, M., C.P. Toret, and D.G. Drubin. 2006. Harnessing actin dynamics for clathrin-mediated endocytosis. *Nat. Rev. Mol. Cell Biol.* 7:404–414. doi:10.1038/nrm1940

Kaneko, T., A. Maeda, M. Takefuji, H. Aoyama, M. Nakayama, S. Kawabata, Y. Kawano, A. Iwamatsu, M. Amano, and K. Kaibuchi. 2005. Rho mediates endocytosis of epidermal growth factor receptor through phosphorylation of endophilin A1 by Rho-kinase. *Genes Cells.* 10:973–987. doi:10.1111/j.1365-2443.2005.00895.x

Keller, R. 2005. Cell migration during gastrulation. *Curr. Opin. Cell Biol.* 17:533–541. doi:10.1016/j.ceb.2005.08.006

Kim, M.H., J. Choi, J. Yang, W. Chung, J.H. Kim, S.K. Paik, K. Kim, S. Han, H. Won, Y.S. Bae, et al. 2009. Enhanced NMDA receptor-mediated synaptic transmission, enhanced long-term potentiation, and impaired learning and memory in mice lacking IRSp53. *J. Neurosci.* 29:1586–1595. doi:10.1523/JNEUROSCI.4306-08.2009

Kirchhausen, T., E. Macia, and H.E. Pelish. 2008. Use of dynasore, the small molecule inhibitor of dynamin, in the regulation of endocytosis. *Methods Enzymol.* 438:77–93. doi:10.1016/S0076-6879(07)38006-3

Kopfstein, L., and G. Christofori. 2006. Metastasis: cell-autonomous mechanisms versus contributions by the tumor microenvironment. *Cell. Mol. Life Sci.* 63:449–468. doi:10.1007/s00018-005-5296-8

Kunwar, P.S., D.E. Siekhaus, and R. Lehmann. 2006. In vivo migration: a germ cell perspective. *Annu. Rev. Cell Dev. Biol.* 22:237–265. doi:10.1146/annurev.cellbio.22.010305.103337

Lee, S.H., F. Kerff, D. Chereau, F. Ferron, A. Klug, and R. Dominguez. 2007. Structural basis for the actin-binding function of missing-in-metastasis. *Structure.* 15:145–155. doi:10.1016/j.str.2006.12.005

Lee, Y.G., J.A. Macoska, S. Korenchuk, and K.J. Pienta. 2002. MIM, a potential metastasis suppressor gene in bladder cancer. *Neoplasia.* 4:291–294. doi:10.1038/sj.neo.7900231

Lin, J., J. Liu, Y. Wang, J. Zhu, K. Zhou, N. Smith, and X. Zhan. 2005. Differential regulation of cortactin and N-WASP-mediated actin polymerization by missing in metastasis (MIM) protein. *Oncogene*. 24:2059–2066. doi:10.1038/sj.onc.1208412

Liu, Y., and D.J. Montell. 1999. Identification of mutations that cause cell migration defects in mosaic clones. *Development.* 126:1869–1878.

Lynch, D.K., S.C. Winata, R.J. Lyons, W.E. Hughes, G.M. Lehrbach, V. Wasinger, G. Corthals, S. Cordwell, and R.J. Daly. 2003. A Cortactin-CD2-associated protein (CD2AP) complex provides a novel link between epidermal growth factor receptor endocytosis and the actin cytoskeleton. *J. Biol. Chem.* 278:21805–21813. doi:10.1074/jbc.M211407200

Ma, S., X.Y. Guan, T.K. Lee, and K.W. Chan. 2007. Clinicopathological significance of missing in metastasis B expression in hepatocellular carcinoma. *Hum. Pathol.* 38:1201–1206. doi:10.1016/j.humpath.2007.01.004

Machesky, L.M., and S.A. Johnston. 2007. MIM: a multifunctional scaffold protein. *J. Mol. Med.* 85:569–576. doi:10.1007/s00109-007-0207-0

Mattila, P.K., M. Salminen, T. Yamashiro, and P. Lappalainen. 2003. Mouse MIM, a tissue-specific regulator of cytoskeletal dynamics, interacts with ATP-actin monomers through its C-terminal WH2 domain. *J. Biol. Chem.* 278:8452–8459. doi:10.1074/jbc.M212113200

Mattila, P.K., A. Pykäläinen, J. Saarikangas, V.O. Paavilainen, H. Vihinen, E. Jokitalo, and P. Lappalainen. 2007. Missing-in-metastasis and IRSp53 deform PI(4,5)P2-rich membranes by an inverse BAR domain-like mechanism. *J. Cell Biol.* 176:953–964. doi:10.1083/jcb.200609176

Miki, H., H. Yamaguchi, S. Suetsugu, and T. Takenawa. 2000. IRSp53 is an essential intermediate between Rac and WAVE in the regulation of membrane ruffling. *Nature.* 408:732–735. doi:10.1038/35047107

Minina, S., M. Reichman-Fried, and E. Raz. 2007. Control of receptor internalization, signaling level, and precise arrival at the target in guided cell migration. *Curr. Biol.* 17:1164–1172. doi:10.1016/j.cub.2007.05.073

Montell, D.J. 2006. The social lives of migrating cells in *Drosophila*. *Curr. Opin. Genet. Dev.* 16:374–383. doi:10.1016/j.gde.2006.06.010

Orth, J.D., E.W. Krueger, S.G. Weller, and M.A. McNiven. 2006. A novel endocytic mechanism of epidermal growth factor receptor sequestration and internalization. *Cancer Res.* 66:3603–3610. doi:10.1158/0008-5472.CAN-05-2916

Palamidessi, A., E. Frittoli, M. Garré, M. Faretta, M. Mione, I. Testa, A. Diaspro, L. Lanzetti, G. Scita, and P.P. Di Fiore. 2008. Endocytic trafficking of Rac is required for the spatial restriction of signaling in cell migration. *Cell.* 134:135–147. doi:10.1016/j.cell.2008.05.034

Patel, A.M., L.S. Incognito, G.L. Schechter, W.J. Wasilenko, and K.D. Somers. 1996. Amplification and expression of EMS-1 (cortactin) in head and neck squamous cell carcinoma cell lines. *Oncogene.* 12:31–35.

Prasad, M., and D.J. Montell. 2007. Cellular and molecular mechanisms of border cell migration analyzed using time-lapse live-cell imaging. *Dev. Cell.* 12:997–1005. doi:10.1016/j.devcel.2007.03.021

Ren, G., P. Vajjhala, J.S. Lee, B. Winsor, and A.L. Munn. 2006. The BAR domain proteins: molding membranes in fission, fusion, and phagy. *Microbiol. Mol. Biol. Rev.* 70:37–120. doi:10.1128/MMBR.70.1.37-120.2006

Rørth, P. 2002. Initiating and guiding migration: lessons from border cells. *Trends Cell Biol.* 12:325–331. doi:10.1016/S0962-8924(02)02311-5

Rørth, P. 2007. Collective guidance of collective cell migration. *Trends Cell Biol.* 17:575–579. doi:10.1016/j.tcb.2007.09.007

Saarikangas, J., J. Hakanen, P.K. Mattila, M. Grumet, M. Salminen, and P. Lappalainen. 2008. ABBA regulates plasma-membrane and actin dynamics to promote radial glia extension. *J. Cell Sci.* 121:1444–1454. doi:10.1242/jcs.027466

Saarikangas, J., H. Zhao, A. Pykäläinen, P. Laurinmäki, P.K. Mattila, P.K. Kinnunen, S.J. Butcher, and P. Lappalainen. 2009. Molecular mechanisms of membrane deformation by I-BAR domain proteins. *Curr. Biol.* 19:95–107. doi:10.1016/j.cub.2008.12.029

Sawallisch, C., K. Berhörster, A. Disanza, S. Mantoani, M. Kintscher, L. Stoenica, A. Dityatev, S. Sieber, S. Kindler, F. Morellini, et al. 2009. The insulin receptor substrate of 53 kDa (IRSp53) limits hippocampal synaptic plasticity. *J. Biol. Chem.* 284:9225–9236. doi:10.1074/jbc.M808425200

Schmidt, M.H., F.B. Furnari, W.K. Cavenee, and O. Bögler. 2003. Epidermal growth factor receptor signaling intensity determines intracellular protein interactions, ubiquitination, and internalization. *Proc. Natl. Acad. Sci. USA.* 100:6505–6510. doi:10.1073/pnas.1031790100

Scita, G., S. Confalonieri, P. Lappalainen, and S. Suetsugu. 2008. IRSp53: crossing the road of membrane and actin dynamics in the formation of membrane protrusions. *Trends Cell Biol.* 18:52–60. doi:10.1016/j.tcb.2007.12.002

Somogyi, K., and P. Rørth. 2004. Cortactin modulates cell migration and ring canal morphogenesis during *Drosophila* oogenesis. *Mech. Dev.* 121:57–64. doi:10.1016/j.mod.2003.10.003

Soubeyran, P., K. Kowanetz, I. Szymkiewicz, W.Y. Langdon, and I. Dikic. 2002. Cbl-CIN85-endophilin complex mediates ligand-induced downregulation of EGF receptors. *Nature.* 416:183–187. doi:10.1038/416183a

Suetsugu, S., K. Murayama, A. Sakamoto, K. Hanawa-Suetsugu, A. Seto, T. Oikawa, C. Mishima, M. Shirouzu, T. Takenawa, and S. Yokoyama. 2006. The RAC binding domain/IRSp53-MIM homology domain of IRSp53 induces RAC-dependent membrane deformation. *J. Biol. Chem.* 281:35347–35358. doi:10.1074/jbc.M606814200

Taipale, J., J.K. Chen, M.K. Cooper, B. Wang, R.K. Mann, L. Milenkovic, M.P. Scott, and P.A. Beachy. 2000. Effects of oncogenic mutations in Smoothened and Patched can be reversed by cyclopamine. *Nature.* 406:1005–1009. doi:10.1038/35023008

Tekotte, H., D. Tollervey, and I. Davis. 2007. Imaging the migrating border cell cluster in living *Drosophila* egg chambers. *Dev. Dyn.* 236:2818–2824. doi:10.1002/dvdy.21305

Teodorof, C., J.I. Bae, S.M. Kim, H.J. Oh, Y.S. Kang, J. Choi, J.S. Chun, and W.K. Song. 2009. SPIN90-IRSp53 complex participates in Rac-induced membrane ruffling. *Exp. Cell Res.* 315:2410–2419. doi:10.1016/j.yexcr.2009.05.010

Timpson, P., D.K. Lynch, D. Schramek, F. Walker, and R.J. Daly. 2005. Cortactin overexpression inhibits ligand-induced down-regulation of the epidermal growth factor receptor. *Cancer Res.* 65:3273–3280.

Timpson, P., A.S. Wilson, G.M. Lehrbach, R.L. Sutherland, E.A. Musgrove, and R.J. Daly. 2007. Aberrant expression of cortactin in head and neck squamous cell carcinoma cells is associated with enhanced cell proliferation and resistance to the epidermal growth factor receptor inhibitor gefitinib. *Cancer Res.* 67:9304–9314. doi:10.1158/0008-5472.CAN-07-0798

Uezu, A., A. Horiuchi, K. Kanda, N. Kikuchi, K. Umeda, K. Tsujita, S. Suetsugu, N. Araki, H. Yamamoto, T. Takenawa, and H. Nakanishi. 2007. SGIP1alpha is an endocytic protein that directly interacts

with phospholipids and Eps15. *J. Biol. Chem.* 282:26481–26489. doi:10.1074/jbc.M703815200

Verstreken, P., T. Ohyama, and H.J. Bellen. 2008. FM 1-43 labeling of synaptic vesicle pools at the *Drosophila* neuromuscular junction. *Methods Mol. Biol.* 440:349–369. doi:10.1007/978-1-59745-178-9_26

Wang, Y., J. Liu, E. Smith, K. Zhou, J. Liao, G.Y. Yang, M. Tan, and X. Zhan. 2007. Downregulation of missing in metastasis gene (MIM) is associated with the progression of bladder transitional carcinomas. *Cancer Invest.* 25:79–86. doi:10.1080/07357900701205457

Woodings, J.A., S.J. Sharp, and L.M. Machesky. 2003. MIM-B, a putative metastasis suppressor protein, binds to actin and to protein tyrosine phosphatase delta. *Biochem. J.* 371:463–471. doi:10.1042/BJ20021962

Yang, C., M. Hoelzle, A. Disanza, G. Scita, and T. Svitkina. 2009. Coordination of membrane and actin cytoskeleton dynamics during filopodia protrusion. *PLoS One.* 4:e5678. doi:10.1371/journal.pone.0005678

Zhu, J., D. Yu, X.C. Zeng, K. Zhou, and X. Zhan. 2007. Receptor-mediated endocytosis involves tyrosine phosphorylation of cortactin. *J. Biol. Chem.* 282:16086–16094. doi:10.1074/jbc.M701997200